Available online at www.sciencedirect.com

SCIENCE DIRECT®

Powder Technology 156 (2005) 213 – 225

POWDER TECHNOLOGY

www.elsevier.com/locate/powtec

Solution technique for a multi-dimensional population balance model describing granulation processes

Charles David Immanuel[a,b], Francis Joseph Doyle III[b,*]

[a]Department of Chemical Engineering, Imperial College London, London SW7 2AZ, United Kingdom
[b]Department of Chemical Engineering, University of California at Santa Barbara, Santa Barbara, CA 93106, United States

Available online 23 May 2005

Abstract

An efficient and novel solution technique is presented for solving multi-dimensional population balance models. In addition to overcoming stiffness in the original system, the algorithm also reduces the computational load by proposing a priori semi-analytical solutions for a major part of the aggregation quadratures (calculations performed once at the start of the simulation). The new technique gives very good solution times, thereby removing the bottleneck from the computational method in the development of detailed population balance-based models for such complex processes. As the emphasis is on the numerical solution technique, simpler forms of the aggregation kernel are employed in the study. However, these kernels reveal crucial information for the optimization and control of the granulation process.

Keywords: Multi-dimensional population balance; Numerical solution; Granulation; Aggregation kernels

1. Introduction and background

Granulation is a particle design process in which fine powdery solids are formed into larger, free-flowing granules. It finds application in a wide range of industries spanning pharmaceuticals, fertilizers, detergents, food processing and others. In these processes, granulation is employed to improve such properties as handling, flow properties, controlled dissolution and delivery rates, uniformity in the distribution of multiple solid components, and even taste and aesthetics. At present, granulation processes are operated in a highly inefficient manner, with large recycle ratios within the process (3–4:1, recycle/product) [1]. This is because of the need to maintain specified size ranges for the granules. Granules that are either smaller or larger than the allowable range are recirculated to the process for reprocessing. The large recycle ratio could partly be because of the improper distribution of the binder fluid, which leaves some of the powder unwetted while some are formed into chunks. Also, in batch processing such as in the pharmaceutical industry, it is very important to ensure homogeneity in the granules in terms of the main ingredient and the excepients. Thus, there is a clear need for better process design, operation and control. In addition, typical applications of the granules call for a tight control of the particle size distribution (PSD), motivated by the effect of PSD on the various end-use properties including drug-dissolution rates, flowability, packing density, color and taste.

During the granulation process, the binder fluid wets the dry powder and 'nucleates' new particles, which are loosely held solid grains. The binder-filled/binder-coated particles stick to each other and grow into larger particles. The particles also compact and consolidate due to the mixing in the granulator, during which process the binder fluid in the interior of the particles are brought to the surface. The particles might also be involved in fragmentation, again due to collision with the walls or with the other particles or due to the mixing action. Thus, the granule size distribution is mainly determined by the phenomena of granule nucleation, consolidation and aggregation, and granule breakage [2]. In certain specific applications, such as in the fertilizer industries, there could be a simultaneous crystallization

* Corresponding author. Tel.: +1 805 893 8133; fax: +1 805 893 4731.
E-mail address: doyle@engineering.ucsb.edu (F.J. Doyle III).

0032-5910/$ - see front matter © 2005 Elsevier B.V. All rights reserved.
doi:10.1016/j.powtec.2005.04.013

from solution and an associated layering of the granules with the solids, perhaps due to supersaturation induced by chemical reactions. Layering can also occur through physical processes. Also, the granulation process might involve simultaneous drying of the binder (undesirable), depending upon the temperature of operation. Thus, the process offers a rich blend of unit operations and processes.

The potential design variables at the disposal of the process engineer for optimization and control are the binder spray (including number and location) and mixing rate (tumbling, agitation). The complexity of the process, the low number of potential manipulated variables and the large time delay associated with the process and the downstream units make the control of granulation processes a challenge. Thus, there is a strong need to evaluate the controllability of the process. But at the same time, these challenges also serve as a strong incentive to the application of model-based strategies firstly for the design and optimization, and secondly for the online control of the granulation processes.

Thus, the development of first-principle model for the granulation process assumes importance. A number of studies have been reported on the underlying phenomena that constitute the granulation process, to cite a few [2–4]. Although these mechanisms underlying the granulation process are still being investigated, a mathematical model is well motivated. It will elucidate the behaviour at the microscopic level, based on details and sensitivities at the mesoscopic (equipment) level. It will also aid in the design of appropriate and effective experiments, to be used in the elucidation of the mechanism as well as the identification of the model parameters.

A suitable methodology for modeling the granulation process is through population balances, which account for the nucleation, consolidation (negative growth), aggregation and breakage phenomena [5]. The consolidation process essentially compacts the granules, reducing the granule porosity and thereby increasing the surface binder content of the granules. The aggregation of the granules constitutes the sticking of two granules, perhaps subsequent to their collision. In addition to its dependence on the size of the granules, the sticking capability of the colliding granules also depends on the binder content of these granules, in particular, the availability of binder on the granule surface. Thus, a realistic characterization of the aggregation rate has to account for the granule size (or solid volume), the binder content and the porosity, thereby necessitating three *internal coordinates* to obtain an accurate representation of the process [6]. These three variables can be re-cast as the volume of solid, liquid and gas in the granules. The advantages with this choice of internal coordinates are:

1. the decoupling of the individual mesoscopic processes (aggregation, consolidation, layering, drying, etc.) and
2. the mutually exclusive character of the internal coordinates that substantially improves the solution of the aggregation model.

These issues will be evident as the developments are presented. The corresponding population balance equation with this choice of internal coordinates is given by:

$$\frac{\partial}{\partial t}F(s,l,g,t)+\frac{\partial}{\partial g}\left(F(s,l,g,t)\frac{\mathrm{d}g}{\mathrm{d}t}\right)+\frac{\partial}{\partial s}\left(F(s,l,g,t)\frac{\mathrm{d}s}{\mathrm{d}t}\right)+\frac{\partial}{\partial l}\left(F(s,l,g,t)\frac{\mathrm{d}l}{\mathrm{d}t}\right)=\Re_{\mathrm{aggre}}+\Re_{\mathrm{break}}+\Re_{\mathrm{nuc}} \quad (1)$$

where $F(s,l,g,t)$ is the population density function, defined such that $F(s,l,g,t)\mathrm{d}s\mathrm{d}l\mathrm{d}g$ is the moles of granules of solid volume between s and $s+\mathrm{d}s$, liquid volume between l and $l+\mathrm{d}l$, and gas volume between g and $g+\mathrm{d}g$. $\Re_{\mathrm{nuc}}(s,l,g,t)$ accounts for the rate of nucleation of new granules. $\Re_{\mathrm{aggre}}(s,l,g,t)$ account for the gain/loss of granules due to the aggregation process, while $\Re_{\mathrm{break}}(s,l,g,t)$ comprises similar terms due to granule breakage. The partial derivative with respect to g on the left hand side accounts for the consolidation phenomenon, wherein $\mathrm{d}g/\mathrm{d}t$ is negative (there is a continuous decrease in the pore volume of the granules as they compact, while the solid and liquid content of each granule is left unaltered). Likewise, the partial derivative term with respect to s accounts for simultaneous crystallization and the layering of the granule surface with the solid, while the term with respect to l accounts for drying effects. These latter two terms are usually restricted to a few special cases. Thus, it is easy to see the decoupling of the individual unit operations and its advantage in the development of population balance models.

One major challenge in developing population balance models in general is the identification of appropriate kernels for the sub-processes (aggregation, breakage, etc.)—the so-called inverse problem. These kernels are not only size-dependent, but are also time varying, being dependent upon the reaction environment. The understanding of the process mechanisms (which are usually in the form of steady state information) have to be appropriately converted into dynamic mathematical representations, which proves to be a non-trivial task in contrast to the development of conventional rate constants for lumped systems. However, studies addressing the development of the mechanistic kernels are appearing in the literature, for aggregation mainly but also for breakage.

Another major rate-limiting step in utilizing these models is the development of efficient solution techniques for the complex multi-dimensional population balance models. Several other practical systems of interest, in addition to the granulation system, require a multi-dimensional formulation for good characterization. Thus, it is of interest to develop a robust, efficient and realistic solution technique for multi-dimensional population balance equations, eliciting interest from several researchers [7–11]. In a thorough study, Mantzaris et al.

[8–10] evaluate the three major solution techniques based on the finite difference technique, the Galerkin's methods and the finite element techniques to solve a two-dimensional population balance model. For the simulation of a typical 2-h batch, they report simulation times of 31 min based on a finite differencing method, 69 min based on the spectral method and 89 min based on a finite element-based collocation method. Several other studies utilize the probabilistic Monte Carlo techniques to solve these complex problems. Wauters [12] solved a three-dimensional model by employing an extension of the technique that has been employed by other authors [13] for solving one-dimensional population balance models. A more rigorous molecular dynamic solution strategy was recently presented by Gantt and Gatzke [14] for this problem.

This paper presents a novel and robust strategy for the solution of a three-dimensional population balance model for the granulation system. The algorithm is based on the technique presented elsewhere for a single dimensional population balance model [15]. Two different forms of aggregation kernels are considered. The main objective of this study is to remove the bottleneck in the model development effort from the computational aspects.

2. Model features

As indicated above, the process of evolution of the granule PSD is determined by the interplay of the subprocesses of nucleation, consolidation, aggregation, breakage and sometimes layering. Two different types of the nucleation phenomena have been identified, subject to the conditions (or regime) of operation of the process [2,3]. These depend upon the powder wetting characteristics, the binder spray rate and the bed mixing rate, and are termed the droplet-controlled regime and the mechanical dispersion regime. In the former regime, each binder droplet results in a separate well-formed granule nucleii, while, in the latter case, multiple droplets coalese onto the dry powder that then gets broken into smaller nucleii due to mechanical dispersion forces. A mechanistic kernel can be developed for the former process (in terms of the binder spray rate, the powder turn-over rate, the nozzle characteristics and the penetration time of the binder fluid into the dry powder). The latter case is similar to the breakage process and very limited information is available to model this using first principles.

The consolidation phenomenon accounts for the compaction of the granules and the associated decrease in the particle porosity. The particle porosity ε is defined as $\varepsilon=(l+g)/(s+l+g)$, which is modeled using heuristic information as shown in Eq. (2). In this equation, the constant c has been found to be dependent upon the mixing rate or tumbling rate in the granulator although no clear correlations have been established. Substituting the definition of ε, this equation can be simplified to Eq. (3) for the rate of decrease in the volume of gas (pores) in the granules [6].

$$\frac{\mathrm{d}\varepsilon}{\mathrm{d}t} = -c(\varepsilon-\varepsilon_{\min}) \tag{2}$$

$$\frac{\mathrm{d}g}{\mathrm{d}t} = -c\frac{(s+l+g)(1-\varepsilon_{\min})}{s}\left[l-\frac{\varepsilon_{\min}s}{1-\varepsilon_{\min}}+g\right]. \tag{3}$$

The formation and depletion terms associated with the aggregation phenomenon are defined in Eqs. (4)–(6) [5]. In these equations, s_{nuc} is the solid volume of nucleii (assumed fixed) and $\beta(s_1,s_2,l_1,l_2,g_1,g_2)$ is the size-dependent aggregation kernel that signifies the rate constant for aggregation of different granules of internal coordinates (s_1,l_1,g_1) and (s_2,l_2,g_2).

$$\mathfrak{R}_{\mathrm{aggre}}(s,l,g,t) = \mathfrak{R}_{\mathrm{aggre}}^{\mathrm{formation}} - \mathfrak{R}_{\mathrm{aggre}}^{\mathrm{depletion}} \tag{4}$$

$$\begin{aligned}\mathfrak{R}_{\mathrm{aggre}}^{\mathrm{formation}} = \frac{1}{2}\int_{s'=s_{\mathrm{nuc}}}^{s-s_{\mathrm{nuc}}}\int_{l'=0}^{l}\int_{g'=0}^{g}\beta\left(s',s-s',l',l-l'\right.\\ \left.-l',g',g-g'\right)F\left(s',l',g',t\right)\\ \times F\left(s-s',l-l',g-g',t\right)\mathrm{d}s'\,\mathrm{d}l'\,\mathrm{d}g'\end{aligned} \tag{5}$$

$$\begin{aligned}\mathfrak{R}_{\mathrm{aggre}}^{\mathrm{depletion}} = F(s,l,g,t)\int_{s'=s_{\mathrm{nuc}}}^{s_{\max}}\int_{l'=0}^{l_{\max}}\int_{g'=0}^{g_{\max}}\beta\left(s',s,l',l,g',g\right)\\ \times F\left(s',l',g',t\right)\mathrm{d}s'\,\mathrm{d}l'\,\mathrm{d}g'\end{aligned} \tag{6}$$

As is common in the previous granulation modeling studies, the turn-over or mixing rate in the granulator is assumed to be high enough to justify the application of the law of mass action in modeling the collision rate in Eqs. (5) and (6).

2.1. Mechanistic aggregation kernel

As indicated earlier, a primary challenge in the development of detailed process models is the understanding of the mechanisms underlying the process and the development of appropriate mathematical representation for the same. This challenge is particularly pronounced in the development of the kernels required in the population balance models. While the development of a multi-dimensional population model is warranted by the physics of the problem, it is a bigger challenge to obtain the required three-dimensional kernels, accounting for the dependence of the rates of the different phenomena on both the particle size and the binder content. However, very good progress has been made in this regard for various systems. For instance, for the emulsion polymerization process, detailed fundamental models of the coagulation process have been developed (see for instance Immanuel et al. [16]). Usually, such fundamental models involve a number of parameters that are either unknown or uncertain. These parameters are fitted to macroscopic

experimental data (on, say, the particle size distribution) employing the full population balance model. This approach serves as the best alternative to the determination of the model parameters based on detailed experiments at the mesocopic levels, which are either expensive or not well developed.

The modeling of the kernels requires the identification of the net attraction potentials (energies) between the different particle pairs. Fig. 1 shows a schematic representation of the aggregation phenomenon for a typical wet granulation process. In the granulation process, the kinetic energy of the particles constitutes the major potential of attraction between the granules ($mu_0^2/2$) [2,4,17]. The dissipation of the kinetic energy of the granules is primarily attributed to the viscous forces in the liquid binder film. Other forces that contribute to the dissipation are the collision energy and the elastic energy of the granules, which come into play only when the particles are involved in an actual collision by overcoming the viscous dissipation. Different forces become important in different regimes of particle sizes, binder content and operating conditions (mixing rates). The capillary repulsive forces between the particles are usually neglected in relation to the stronger viscous forces.

The particles that approach each other as a result of their kinetic energy will either coalesce or rebound. Coalescence is classified into two types—type I and type II. Type I coalescence occurs when the viscous force is able to overcome the kinetic energy, causing the particles to coalesce before the occurrence of a collision (through the liquid bridge). Type II coalescense occurs when the particles actually collide with each other. The collision causes particle deformation, which results in the release of the elastic energy of the particles thereby causing the particles to retract. If the released elastic energy is dissipated in the viscous layer, then type II coalescence occurs. If all the elastic energy is not dissipated, then the particles rebound.

Net attractive potential for type I coalescence (balancing the kinetic energy with the viscous repulsion) is given by

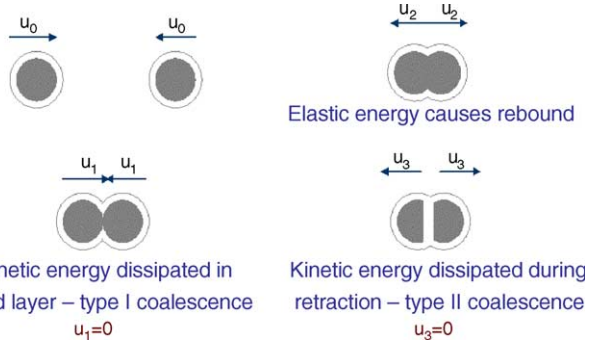

Fig. 1. Schematic representation of the two types of aggregation phenomena ([2,4]). u_0 is the approach velocity at infinite separation; u_1 is the velocity at impact; u_2 is the initial rebound velocity; u_3 is the velocity at the separation of binder layers.

Eq. (7), where p_1 and p_2 are the two particles, m is the reduced mass of the particles, h is the separation distance between the particles and u is the varying relative velocity of the particles as they approach each other [2,4]. The velocity u is given by Eq. (8), wherein h_0 is the depth of the liquid binder film on the surface, u_0 is the initial approach velocity of the particles (based on the mixing rates in the granulator) and St_v is the viscous Stokes' number.

$$\psi(p_1,p_2,h) = \frac{1}{2}m(2u(h))^2 \tag{7}$$

$$u = u_0,\ h > h_0$$

$$u = u_0\left[1 - \frac{1}{St_v}\ln\left(\frac{h_0}{h_a}\right)\right],\ h < h_0 \tag{8}$$

For type II coalescence, two different sequential processes are involved—the forward and the reverse paths. The process with the higher energetics is the rate-determining process. The net attractive potential for the two processes is given in Eqs. (9) and (10), where E_c is the energy lost during impact and deformation, given in Eq. (11), u_1 being the velocity at impact calculated from Eq. (8). The net rebound velocity u' is defined in Eqs. (12) and (13), δ'' being the permanent plastic deformation in the granules [2,4].

$$\psi_{\text{forward}}(p_1,p_2,h) = \frac{1}{2}m(2u(h))^2 - E_c \tag{9}$$

$$\psi_{\text{reverse}}(p_1,p_2,h) = -\frac{1}{2}m\left(2u'\right)^2 \tag{10}$$

$$E_c = \frac{1}{2}m(2u_1)^2 \tag{11}$$

$$u'(h) = u_2 - \frac{3\pi\mu\tilde{D}^2}{16\tilde{m}h^2}\left[\left(\delta''\right)^2\left(\frac{h^2}{h_a^2} - 1\right) + 2h\delta''\left(\frac{h}{h_a} - 1\right) + 2h^2\ln\left(\frac{h}{h_a}\right)\right],\ 0 < h < h_0$$

$$u'(h) = u'(h_0),\ h > h_0 \tag{12}$$

$$\delta'' = \left(\frac{8}{3\pi}\right)^{\frac{1}{2}}(St_{\text{def}})^{\frac{1}{2}}\tilde{D}\left[1 - \frac{1}{St_v}\ln\left(\frac{h_0}{h_a}\right)\right] \times \left[1 - 7.36\frac{Y_d}{E^*}(St_{\text{def}})^{-\frac{1}{4}}\left[1 - \frac{1}{St_v}\ln\left(\frac{h_0}{h_a}\right)\right]^{-\frac{1}{2}}\right] \tag{13}$$

These steady state forces can be incorporated into a dynamic calculation of the aggregation rates and the aggregation kernel, as described in the emulsion polymerization literature [16]. These net attractive potential information can be employed in the Smoluchowski formulation as shown in Eq. (14). The Fuch stability ratio W is defined

in Eqs. (15) and (16) for type I and type II aggregation, respectively. In these equations, r_i is the radius of particle p_i, k is the Boltzmann constant, T is the temperature and c_1 is an adjustable constant.

$$\beta(p_1,p_2) = c_1 \frac{4\pi u_0 (r_1+r_2)^2}{W} \tag{14}$$

$$W(p_1,p_2) = (r_1+r_2)\int_{D=(r_1+r_2)}^{\infty} \frac{\exp\left(\frac{\psi(p_1,p_2,D)}{kT}\right)}{D^2} d(D) \tag{15}$$

$$\frac{W(p_1,p_2)}{r_1+r_2} = \max\left(\int_{D=(r_1+r_2)}^{\infty} \frac{\exp\left(\frac{-\psi_{\text{forward}}(p_1,p_2,D-r_1-r_2)}{kT}\right)}{D^2} d(D),\right.$$
$$\left. \times \int_{D=(r_1+r_2)}^{\infty} \frac{\exp\left(\frac{-\psi_{\text{reverse}}(p_1,p_2,D-r_1-r_2)}{kT}\right)}{D^2} d(D)\right) \tag{16}$$

2.2. Empirical aggregation kernels

The primary objective of the study presented here is to develop a robust solution technique for the three-dimensional population balance models. Thus, although the theory presented in the previous subsection can be utilized in predicting the rigorous aggregation kernel, the present study is based on semi-empirical aggregation kernels. Two different representations of the empirical three-dimensional aggregation kernel are considered.

2.2.1. Case 1

As briefly highlighted above, aggregation is dependent upon different regimes of the particle size and the binder content. This information has been converted into simple heuristics for the aggregation kernel [12]. This heuristics identifies the ranges of solid, liquid and gas volumes of the colliding particles that lead to successful aggregation. However, it assigns a constant rate constant for each of these feasible aggregation regimes, not to mention the effect of the different particle sizes and the binder contents within each regime (i.e., $\beta(s_1,s_2,l_1,l_2,g_1,g_2)=\beta_0 P(s_1,s_2,l_1,l_2,g_1,g_2)$, wherein P assumes values of either one or zero). The result is an aggregation kernel which follows an on–off or one-zero pattern. In essence, the ranges of particle variables (internal coordinates) are classified into 'large' or 'small' based on a defined cut-off total volume. Likewise, the particles are classified as 'wet' or 'dry' depending upon the binder content in the particles. Certain permutations and combinations of these particles are assumed to aggregate successfully upon collision, while the rest are assumed to not aggregate. A 'small' and 'wet' granule is assumed to successfully aggregate, upon collision with any other granule. On the other hand, a 'big' and 'dry' granule will aggregate only with a 'small' and 'wet' granule upon collision, and with no other granules. A 'big' and 'wet' granule will successfully aggregate with all but a 'big' and 'dry' granule, while a 'small' and 'dry' granule will not aggregate with another 'dry' granule irrespective of its size range. (See Wauters [12], Table 5.1.)

2.2.2. Case 2

Recently, Madec et al. [18] have presented an empirical expression for the aggregation kernel that accounts for the dependence of the aggregation rate on both the size and the composition of the granules. This expression is given below:

$$\beta(s_1,s_2,l_1,l_2,g_1,g_2) = \beta_1\left(L_1^3+L_2^3\right)\left((c_1+c_2)^{\alpha} \times\left(100-\frac{c_1+c_2}{2}\right)^{\delta}\right)^{\alpha} \tag{17}$$

In the above equation, L_i denotes the diameter of particle i ($L_i=((s_i+l_i+g_i)6/\pi)^{1/3}$); c_i denotes the volume fraction of the liquid in granule $i\left(c_i=\frac{l_i}{s_i+l_i+g_i}\right)$; and β_1, α and δ are parameters. The parameter β_1 could be correlated with the degree of mixing in the granulator. The main disadvantage with this kernel is that it predicts a monotonically increasing aggregation rate with increase in the particle size, which contradicts experimental observations (and the theory presented above). However, the dependence is relatively much weaker on the particle size than on the binder content. Thus, this kernel presents a good starting point to the development of a self-contained multi-dimensional aggregation kernel.

3. Hierarchical two-tier technique

A novel and efficient solution technique was developed for one-dimensional population balance models and applied to an emulsion polymerization application [15]. This technique is based on a finite-element discretization of the particle population and tracks the total particles within each of the bins. The equation representing the total particles within each bin can be derived from the population balance equation in a straight-forward manner (partial analytical solution).

The one-dimensional solution technique gives almost three orders of magnitude improvement in the computation times compared to standard solution techniques. This is achieved partly due to a reduction of the stiffness of the system of equations by a hierarchical decomposition solution strategy. In effect, the population balance equation is reformulated in terms of the individual growth, aggregation, nucleation and breakage events (as appropriate), thereby accommodating the differences in their time scales. The other major factor that contributes to this

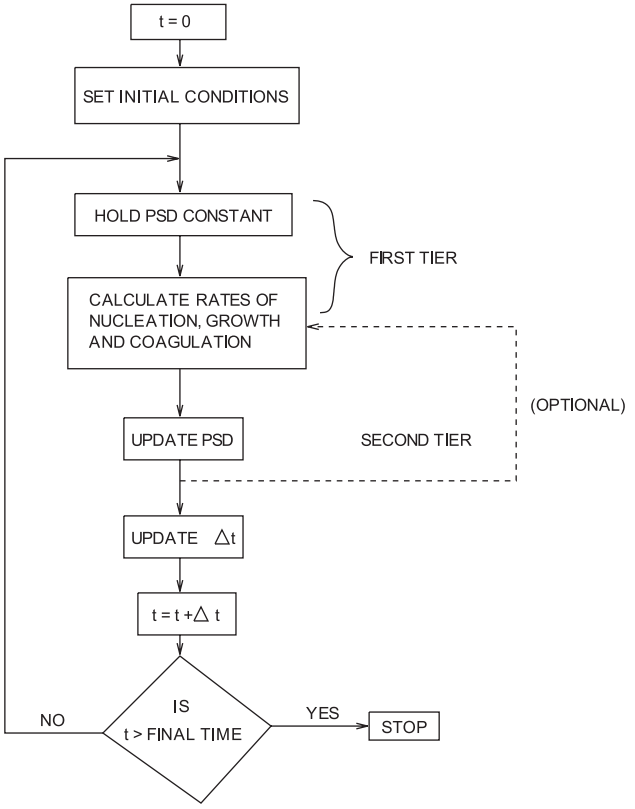

Fig. 2. Schematic representation of the two-tier hierarchical algorithm [15].

improvement in computation time is the offline analytical solution that was proposed for the aggregation quadratures. This results in casting the complex integrals in terms of simpler multiplication and addition, thereby leading to a substantial reduction in the computational load. These analytical solutions for the quadratures are derived based on an assumption of a uniform particle density within each element, although this assumption can be easily relaxed to enable larger finite elements. Fig. 2 shows a schematic of the two-tier algorithm, reproduced from Immanuel and Doyle III [15]. See the original reference for more details on the algorithm and the quasi-analytical solution equations for the quadratures.

Fig. 3 compares the numerical simulation results with pure analytical solutions for an aggregation-only population-balance equation [19]. The initial condition is also shown in the figure. As seen in the figure, the analytical and numerical solutions coincide strongly, validating the quasi-analytical numerical solution technique and its underlying assumption of a uniformity of particle density within each bin.

This one-dimensional algorithm is extended to the multi-dimensional case here. The ranges of volumes of solid, liquid and gas are divided into three-dimensional grids (finite volumes or bins). In this case, the algorithm models the total particle count within each of these bins, defined such that $F_{i,j,k}$ is the total moles of particles within the (i,j,k)th bin (Eq. (18)). The layering effect and the drying effect (which account for the continuous change in the solid and liquid contents of the granules) are neglected in this equation. Thus, continuous growth is restricted to the gas volume (due to consolidation). In this equation, gb_k is the lower boundary of gas volume in the kth bin along the gas volume and Δg_k is the width of the kth bin along the gas volume.

$$\frac{\mathrm{d}}{\mathrm{d}t}F_{i,j,k} + \left(\frac{F_{i,j,k}}{\Delta g_k}\right)\frac{\mathrm{d}g}{\mathrm{d}t}\Big|_{gb_k} - \left(\frac{F_{i,j,k+1}}{\Delta g_{k+1}}\right)\frac{\mathrm{d}g}{\mathrm{d}t}\Big|_{gb_{k+1}} = \int_{s_{i-1}}^{s_i}\int_{l_{i-1}}^{l_i}\int_{g_{i-1}}^{g_i}\Re_{\mathrm{aggre}}(s,l,g,t)\mathrm{d}s\mathrm{d}l\mathrm{d}g \quad (18)$$

Extensions of the analytical solutions for the aggregation integrals to multi-dimensional cases is straightforward. The aggregation term in Eq. (18) assumes a six-dimensional form in the current three-dimensional case ($\Re_{\mathrm{aggre}}$ itself

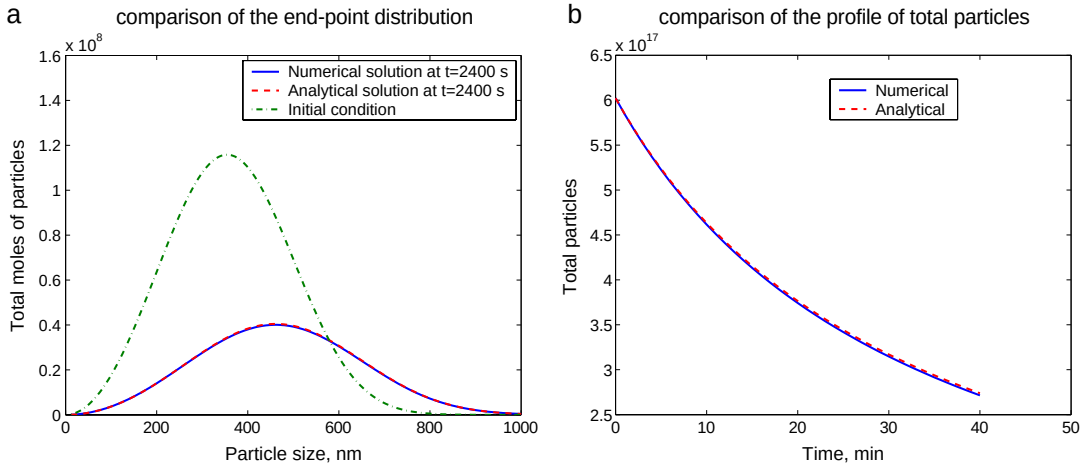

Fig. 3. Comparison of the numerical solution of an aggregation-only population balance equation (based on a quasi-analytical solution for the aggregation integrals subject to the assumption of uniform particle density within each finite element) with a purely analytical solution (for a simplified initial condition).

being a three-dimensional integral, as seen in Eqs. (4)–(6)). This six-dimensional integral can be re-cast as a multiple of three double integrals, each double integral accounting for one internal coordinate. For instance, consider the application of Eq. (18) to a particular element (i,j,k). One term in the integral in the RHS accounts for the rate of formation of particles in bin (i,j,k) by the coalescence of particles in two other smaller bins (i_1,j_1,k_1) and (i_2,j_2,k_2) (see Eqs. (5) and (6)). For the smallest possible bin (i_2,j_2,k_2) that, upon coalescence with bin (i_1,j_1,k_1) results in particles in bin (i,j,k), the rate of formation term in the RHS of Eq. (18) is given by:

$$\begin{aligned}\Re_{\text{formation}}(i,j,k,i_1,j_1,k_1) = {} & \beta_{i_1,j_1,k_1,i_2,j_2,k_2} F_{V,i_1,j_1,k_1} F_{V,i_2,j_2,k_2} \\ & \times \left[\int_{s'=s_{i-1}-s_{i_1}}^{s_i} \int_{s''=s_{i-1}-s'}^{s_{i_1}} \mathrm{d}s'' \mathrm{d}s' \right] \\ & \times \left[\int_{l'=l_{i-1}-l_{i_1}}^{l_i} \int_{l''=l_{i-1}-l'}^{l_{i_1}} \mathrm{d}l'' \mathrm{d}l' \right] \\ & \times \left[\int_{g'=g_{i-1}-g_{i_1}}^{g_i} \int_{g''=g_{i-1}-g'}^{g_{i_1}} \mathrm{d}g'' \mathrm{d}g' \right] \\ & + \cdots \end{aligned} \tag{19}$$

where $F_{V,i,j,k}=F_{i,j,k}/(\Delta s_i \Delta l_j \Delta g_k)$. Refer to Figs. 4 and 5 and the ensuing equations in Ref. [15] for interpretations and equations. In the above equation, s_i is the upper limit in the ith bin along the solid volume, l_j is the upper limit in the jth bin along the liquid volume and g_k is the upper limit in the kth bin along the gas volume. Similarly, Δs_i, Δl_j and Δg_k are the width of the (i,j,k)th bin along the solid, liquid and gas volumes, respectively. The continuation dots is Eq. (19) account for the formation of particles in bin (i,j,k) by coalescence of particles in bin (i_1,j_1,k_1) with other bins (larger than bin (i_2,j_2,k_2)).

The solution to each of the double integrals (within square brackets in Eq. (19)) is the same as the ones derived for the one-dimensional case. This simplification is another advantage of representing the population balance in terms of the volumes of solid, liquid and gas in the granules (rather than in terms of the total particle size, binder content and porosity). Using the individual rates of aggregation and consolidation, the particle population density is updated by the integration of Eq. (18) employing a suitable integration method. A sixth order implicit Simpson's method was used for the aggregation terms and a first order Euler method for the consolidation terms.

4. Simulation results

4.1. Case 1 aggregation kernel

In Figs. 4 and 5, simulation results corresponding to a 2-h batch granulation process are presented. The initial seed consists of granules with an average solid volume of 8.8×10^{-12} m^3, an average liquid volume of 1.6×10^{-17} m^3 and an average gas volume (pore volume) of 4.5×10^{-19} m^3 (all particles in a single bin). The total number of particles in the seed is 6.023×10^{11}, which translates into a total volume of 5.3 m^3. The mixing rate is assumed to be high enough to result in a uniform distribution of the binder among all the particles. Fresh nucleation events are assumed to be absent, with the batch proceeding with pre-formed seed particles. For the simulations, 35 finite elements are employed along solid volume, 15 along the liquid and 12 along the gas (uniformly distributed with respect to radius). Fig. 4 records a modest drop in the total particles and an increase in the average diameter of about 20.5 μm, starting with the initial seed and the initial binder content. The two-dimensional plots of the particle size distribution at the end of the batch, for different values of the gas (pore) volume,

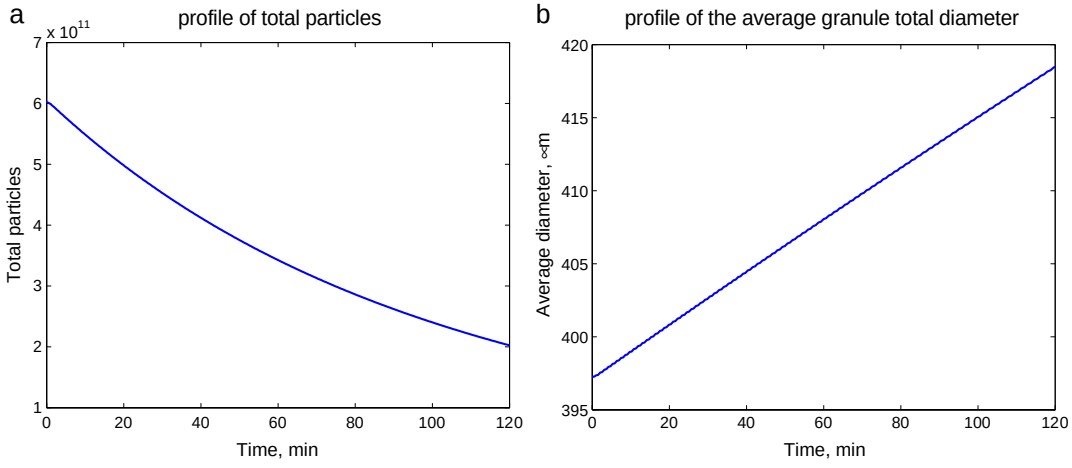

Fig. 4. Typical simulation results for a 2-h granulation process, with case I aggregation kernel.

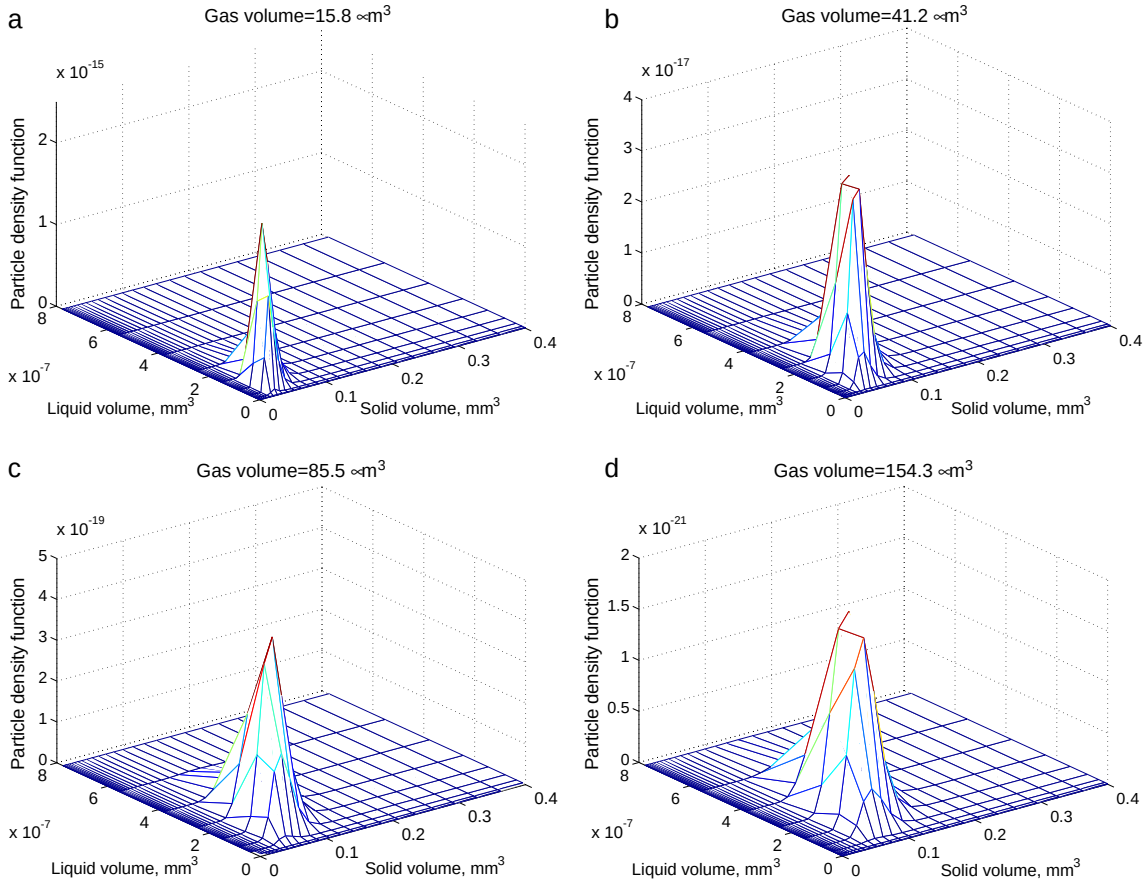

Fig. 5. Snapshots of the end-point particle size distribution at $t=2$ h, for different values of gas volume (of the particles), for case I aggregation kernel. The seed particles are mono-sized.

are shown in Fig. 5. The seed particles (that are all focussed in a single bin) spread with the progress of the batch due to the aggregation and consolidation phenomena. The two-dimensional end-point PSD plots are all near-unimodal. The figure records an exponential decline in the total particles with the gas volume.

In Fig. 6, the sensitivity of the simulation results to the aggregation rate constant β_0 is presented. As seen in the plots, larger values of β_0 leads to larger aggregation rates as expected, thereby resulting in lower total particles and in larger diameters. Similarly, as seen in Fig. 7, as the consolidation rate constant c increases, the compaction rate of the particles increases, thereby increasing the degree of wetness or the fractional binder content of the particles. This in turn increases the aggregation rates and decreases the total particles. However, the average diameter is reduced with increasing c, being dominated by the compaction process than the aggregation process. Note that, beyond $c=5\times10^{-2}$, a saturation effect is observed and there is no further increase in the aggregation rates.

4.2. Case 2 aggregation kernel

Fig. 8 shows the relative aggregation kernel β/β_1 (Eq. (17)) corresponding to a reference particle of total diameter 250μ and binder content 1.8×10^{-4} (corresponding to the seed particles). The plot shows a large drop in the aggregation rate with drop in the binder content of the colliding particle. Also, as pointed out earlier, the kernel predicts an increasing aggregation rate with increase in the diameter of the colliding particle. However, this latter effect is not as pronounced as the effect of the binder content.

Fig. 9 presents batch simulation results corresponding to this aggregation kernel. The values of the parameters α and δ are obtained from the original reference [18] ($\alpha=4.5$ and $\delta=1.125$), while the parameter β_1 is to be utilized as an adjustable parameter. A value of $\beta_1=1\times10^{73}$ is employed. As seen in the plots, the particles in the initial seed undergo aggregation and form a larger mode of particles, thereby resulting in a bimodal distribution at the end of the batch. The formation of the larger mode occurs very rapidly (in less than 1 min—see Fig. 10), and thereafter results in reduced aggregation rates. One reason for this can be inferred from the aggregation kernel (Fig. 8). The new mode of particles are at a much reduced binder content of about 3.0×10^{-6} for which the aggregation rates are very low.

Fig. 10 shows the effect of consolidation on the evolution of the granules. As was observed in the previous case in the parametric sensitivity results, consolidation enhances the aggregation rates and thereby reduces the total particles.

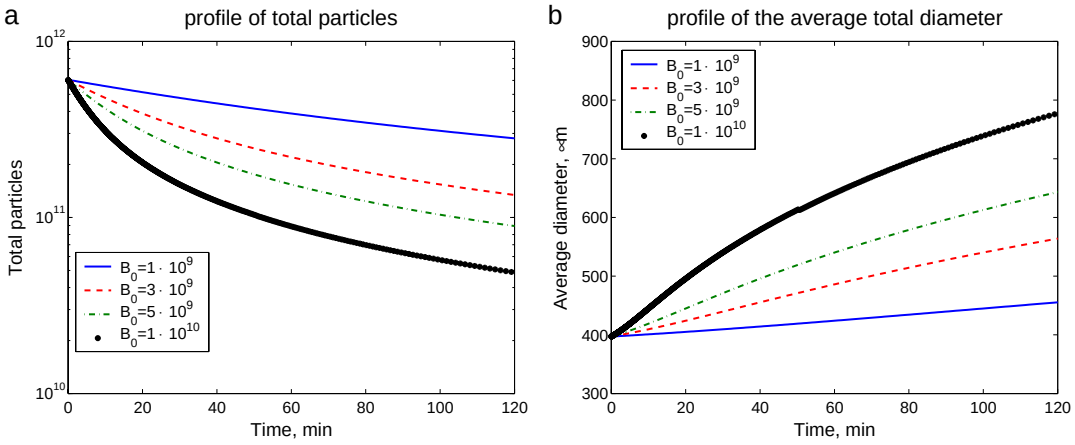

Fig. 6. Parametric sensitivity to the aggregation rate constant β_0.

However, the particles are smaller (more compact), the size being more strongly determined by the consolidation phenomenon than the aggregation phenomenon.

The effect of intermediate addition of the binder on the granulation process are discussed in Figs. 11 and 12. In the one-shot binder addition case, all the intermediate binder is added at 17 min into the batch. On the other hand, in the continuous binder addition case, the binder flow commences at 17 min and continues till 50 min. In both cases, the total amount of intermediate binder is the same. In the plots shown in Fig. 11, a dual effect is observed. The first is the straightforward effect of an increased aggregation rate with addition of binder, as expected. The second is an unexpected drop in the aggregation rates after an initial increase. This latter effect is because of the drop in the binder content after an increase in the total particle size, which in turn is caused by the increased aggregation rates immediately after binder addition. This effect is similar to the effect causing the falling rates observed in the earlier results presented in Figs. 9 and 10, and also in Figs. 4–7 for the case I kernel.

Due to these dual effects, it is seen in Fig. 11 that a continuous spray of binder over a period of time is beneficial over a one-shot addition of the same amount of binder. A one-shot addition results in a momentary increase in the aggregation rates, and hence to a drop in the total particles and an associated increase in the size of the particles. However, the increase in the particle size leads to a reduced (fractional) binder content, thereby not sustaining the increased aggregation rates. For this case, the aggregation rates are found to be the same as in the case without any intermediate binder addition (as evident from the slope of the plot of total particles in Fig. 11(a)). On the other hand, a gradual and continuous addition of the binder results in a prolonged increase in the size of the particles. This removes the nonlinearity in the process that manifested itself as a drop in the binder content in the previous one-shot binder addition. Fig. 12 compares the effect of the two modes of intermediate binder addition on the end-point distribution (shown for two different values of gas volume). It is seen that the particles are depleted from the smaller volume snap shot (compare the range of the z-axis in Fig.

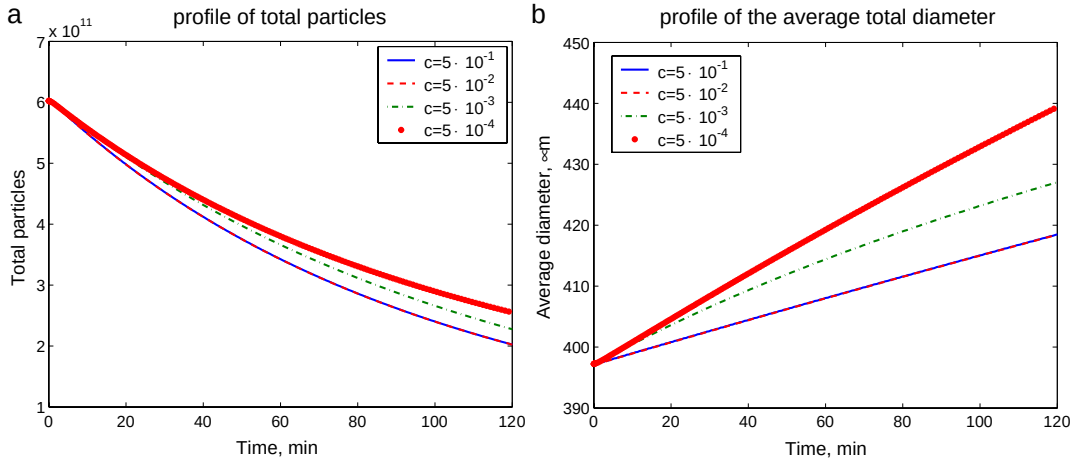

Fig. 7. The effect of consolidation on the evolution of the granules. Note that the plots corresponding to $c=5\times10^{-2}$ and $c=5\times10^{-1}$ merge with each other due to saturation of effects.

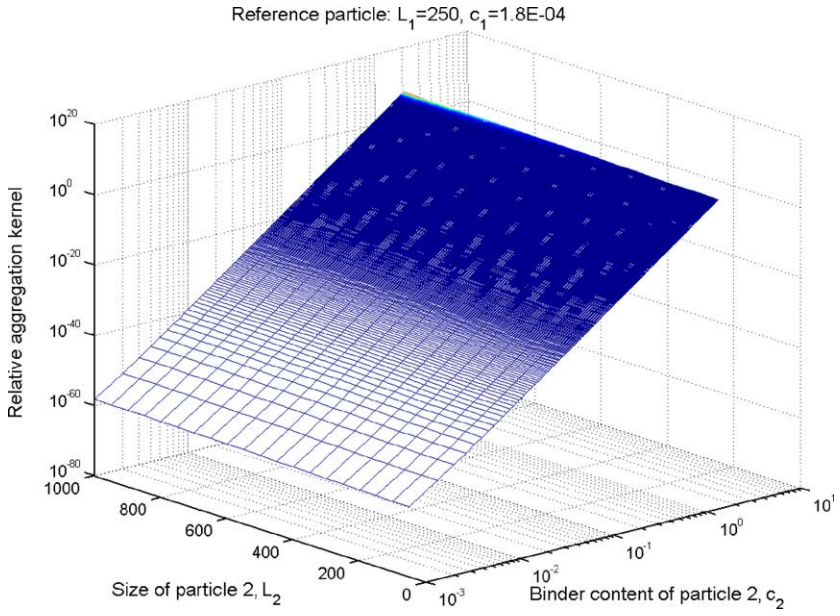

Fig. 8. Aggregation kernel for case 2 (Eq. (17)). Reference particle diameter: $s=250\mu$, $l=3.13\mu$ and $g=0.95\mu$.

12(a), (c) and (e)), with a larger depletion being evident in the continuous addition case (Fig. 12(c)). This shift towards larger sizes is also evident in the snapshots at the higher gas volume (Fig. 12(b), (d) and (f)).

5. Conclusions

An effective and robust technique for the numerical solution of three-dimensional population balance models

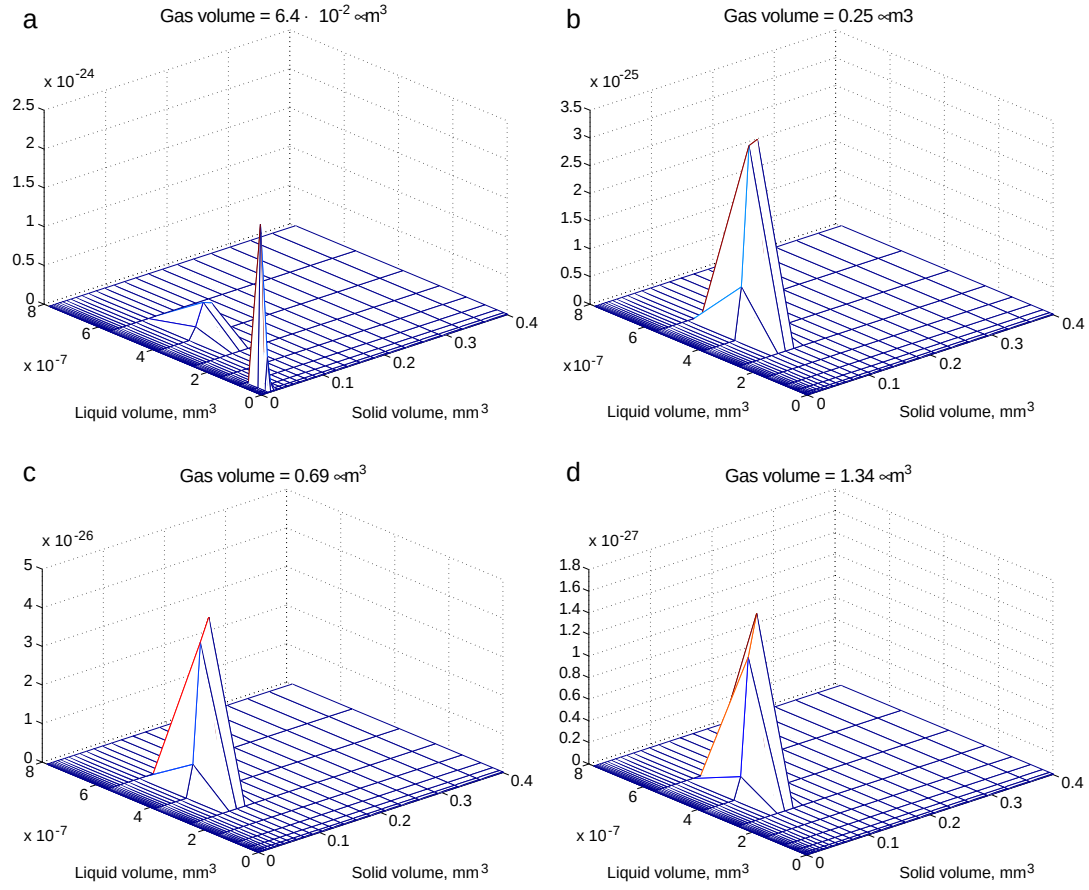

Fig. 9. Snapshots of the end-point particle size distribution at $t=2$ h, for case 2 aggregation kernel. The seed particles are mono-sized.

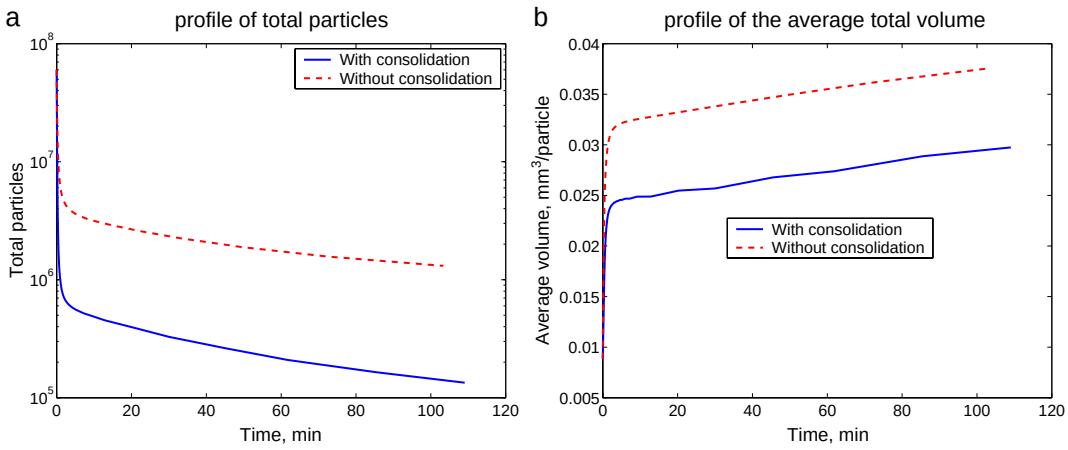

Fig. 10. The effect of consolidation on the evolution of the granules, with case II aggregation kernel.

describing granulation processes was presented. The technique particularly addresses the computational challenge in modelling the three-dimensional aggregation integrals. The technique is an extension of the algorithm presented for a one-dimensional model in previous studies [15]. It is based on a hierarchical two-tier solution strategy, which determines the individual nucleation, growth, aggregation/breakage phenomenon in the first tier of the algorithm, with the updating of the PSD being done in the second tier of the algorithm (in a sequential manner). It was seen in the earlier studies, by comparison with more standard solution techniques, that iteration over the two tiers of the algorithm is not essential. Another significant feature of the proposed solution strategy is the partial a priori solution of the computation-intensive integrals (major portion of the calculations performed once at the start of the simulation). Thus, the application of this hierarchical technique in terms of the individual rates enables a substantial reduction in the computational load.

The application of this technique to the three-dimensional granulation model results in a very efficient computation, with the best simulation time being 15 min for a 2-h batch. An average solution time for a 2-h batch, which varies with the recipe, the model parameters and the aggregation kernel itself, was found to be approximately 1 h. Although literature reports on the solution of multi-dimensional population balances are sparse, the best time reported for the solution of a 3-D population balance model is 111.7 min [9]. The application presented in that case is a biological system wherein the computation-intensive aggregation phenomenon is irrelevant.

In implementing the developed solution technique for multi-dimensional population balance models of granulation processes, the influence of different forms of aggregation kernels were investigated. These kernels serve as precursors to a mechanistic first-principle-based kernel characterizing the aggregation phenomenon. They also reveal several interesting aspects that assume importance for the optimization and control of the process. In particular, the process nonlinearities suggest a need to employ a gradual and prolonged binder spray for control

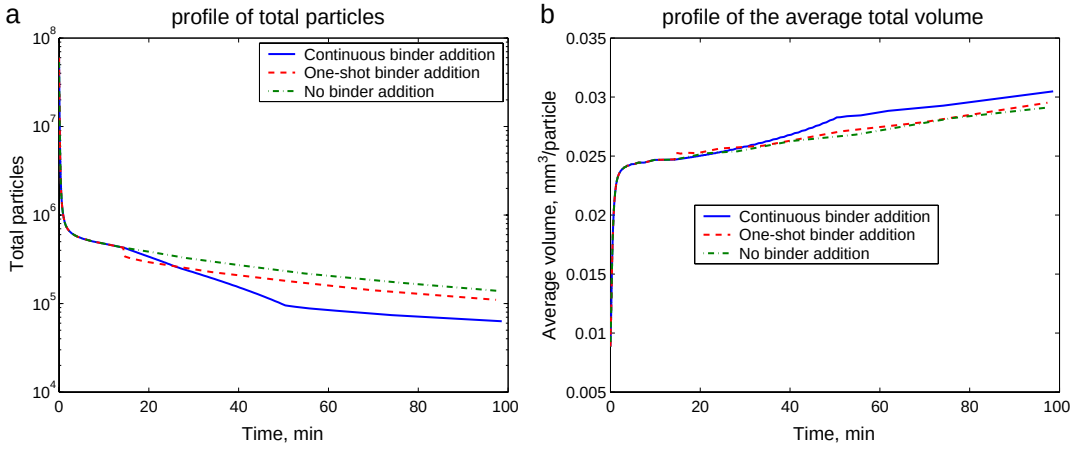

Fig. 11. The effect of intermediate addition of binder on the evolution of the granules—two different modes of intermediate binder addition are studied.

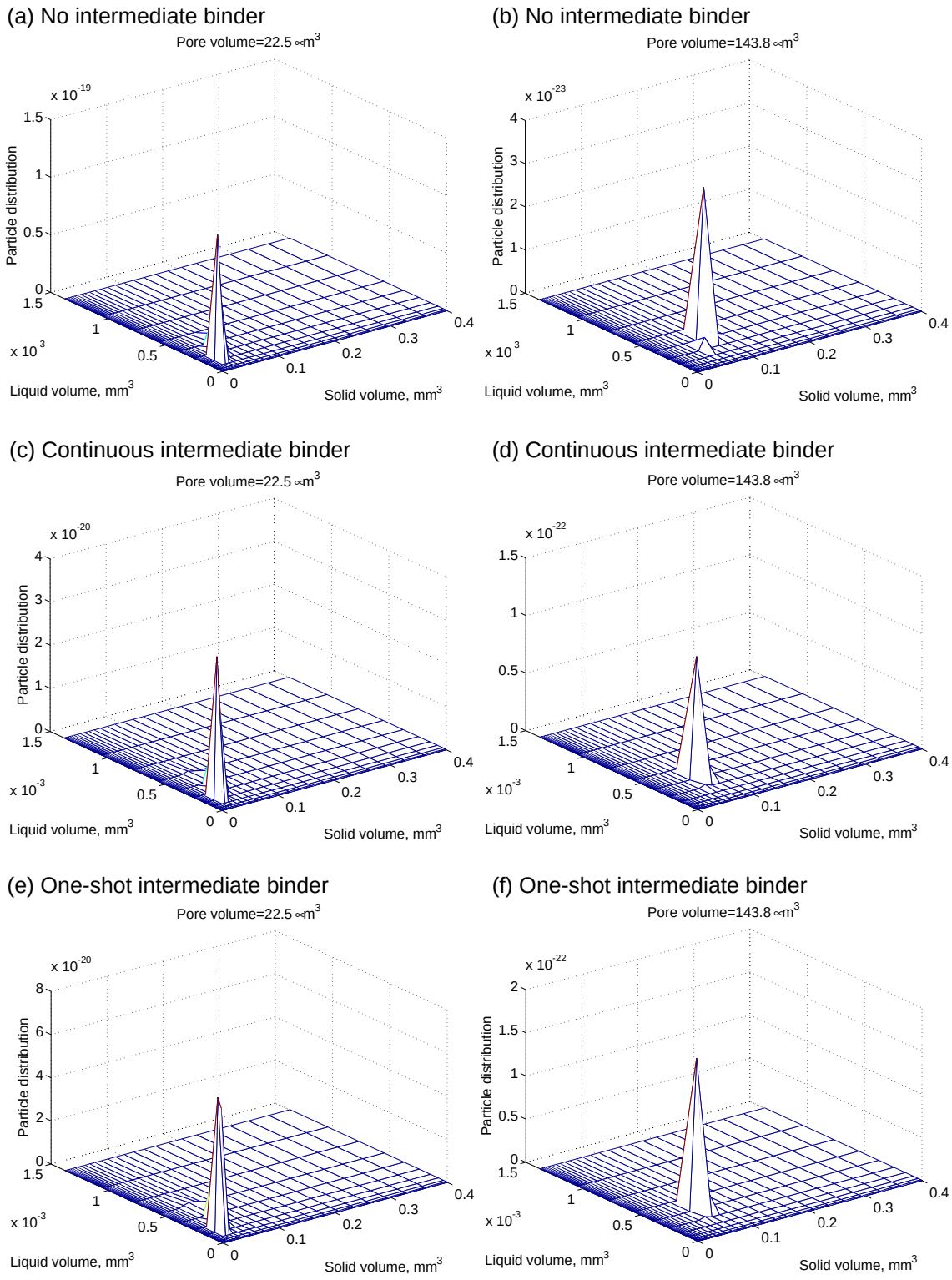

Fig. 12. The effect of intermediate binder addition on the end—point PSD.

of PSD, as opposed to a few one-shot binder additions at different points in the batch (for the same total amount of binder).

The two-tier solution technique renders population-balance model-based optimization studies on the granulation process feasible. However, online applications might necessitate model reduction strategies to be considered. One strategy to tackle this situation would be to consider a three-dimensional population balance model for offline purposes, complemented with a one-dimensional population balance model, based on the overall granule size, for online purposes.

Nomenclature

s	solid volume
l	liquid volume
g	gas volume
$F(s,l,g,t)$	particle density function
$F_{i,j,k}$	total particles in the (i,j,k)th bin
$\Re_{\text{aggre}}$	rate of aggregation
$\Re_{\text{break}}$	rate of breakage
$\Re_{\text{nuc}}$	rate of nucleation
t	time
s_i	representative solid volume in the ith bin along solid volume
l_j	representative liquid volume in the jth bin along liquid volume
g_k	representative gas volume in the kth bin along gas volume
Δs_i	width of ith bin along solid volume
Δl_j	width of jth bin along liquid volume
Δg_k	width of kth bin along gas volume
ε	porosity of the particles
$\varepsilon_{\min}$	minimum porosity of the particles
$\beta(s_1,s_2,l_1,l_2,g_1,g_2)$	aggregation rate constant
c	consolidation rate constant
ψ	net energy of attraction between the particles
p_1	particle number 1
p_2	particle number 2
h	separation distance between two approaching particles
u	net velocity of approach of the particles
u_0	approach velocity at infinite separation distance
u_1	velocity at impact between two particles
δ''	plastic deformation subsequent to collision
St_{v}	Stokes' viscosity
E_{c}	elastic energy of collision
Y_{d}	yield stress
E^*	Young's modulus
St_{def}	Stokes' deformation number
h_0	thickness of binder layer on particle surface
h_{a}	surface asperites on the granules
k	Boltzmann constant
T	granulation temperature
$W(p_1,p_2)$	stability ratio between two particles p_1 and p_2
r_i	(overall) radius of particle i

References

[1] P.R. Mort, S.W. Capeci, J.W. Holder, Control of agglomerate attributes in a continuous binder-agglomeration process, Powder Technol. 117 (2001) 173–176.

[2] S.M. Iveson, J.D. Litster, K. Hapgood, B.J. Ennis, Nucleation, growth and breakage phenomena in agitated wet granulation processes: a review, Powder Technol. 117 (2001) 3–39.

[3] A.A. Adetayo, J.D. Litster, S.E. Pratsinis, B.J. Ennis, Population balance modelling of drum granulation of materials with wide size distribution, Powder Technol. 82 (1995) 37–49.

[4] L.X. Liu, J.D. Litster, A.M. Iveson, B.J. Ennis, Coalescence of deformable granules in wet granulation processes, AIChE J. 46 (2000) 529–539.

[5] D. Ramkrishna, Population Balances, Academic Press, San Diego, 2000.

[6] D. Verkoeijen, G.A. Pouw, G.M.H. Meesters, B. Scarlett, Population balances for particulate processes—a volume approach, Chem. Eng. Sci. 57 (2002) 2287–2303.

[7] D.L. Ma, D.K. Tafti, R.D. Braatz, High resolution simulation of multi-dimensional crystallization, Ind. Eng. Chem. Res. 41 (2002) 6217–6223.

[8] N.V. Mantzaris, P. Daoutidis, F. Srienc, Numerical solution of multi-variable cell population balance models: I. Finite difference methods, Comput. Chem. Eng. 25 (2001) 1411–1440.

[9] N.V. Mantzaris, P. Daoutidis, F. Srienc, Numerical solution of multi-variable cell population balance models: II. Spectral methods, Comput. Chem. Eng. 25 (2001) 1441–1462.

[10] N.V. Mantzaris, P. Daoutidis, F. Srienc, Numerical solution of multi-variable cell population balance models: III. Finite elements methods, Comput. Chem. Eng. 25 (2001) 1463–1481.

[11] M.A. Henson, D. Muller, M. Reuss, Cell population modelling of yeast glycolytic oscillations, Biochem. J. 368 (2002) 433–446.

[12] P.A.L. Wauters, Modelling and mechanisms of granulation. PhD thesis, Department of Chemical Engineering, University of Queensland, Delft University of Technology, The Netherlands, 2001.

[13] K. Lee, T. Matsoukas, Simultaneous coagulation and break-up using constant-n Monte Carlo, Powder Technol. 110 (2000) 82–89.

[14] J.A. Gantt, E.P. Gatzke, High-shear granulation modeling using a discrete element simulation approach, Powder Technol. 156 (2005) 195–212.

[15] C.D. Immanuel, F.J. Doyle III, Computationally-efficient solution of population balance models incorporating nucleation, growth and coagulation, Chem. Eng. Sci. 58 (16) (2003) 3681–3698.

[16] C.D. Immanuel, C.F. Cordeiro, S.S. Sundaram, F.J. Doyle III, Population balance PSD model for emulsion polymerization with steric stabilizers, AIChE J. 49 (6) (2003) 1392–1404.

[17] B.J. Ennis, G. Tardos, R. Pfeffer, A microlevel-based characterization of granulation phenomena, Powder Technol. 65 (1991) 257–272.

[18] L. Madec, L. Falk, E. Plasari, Modelling of the agglomeration in suspension process with multidimensional kernels, Powder Technol. 130 (2003) 147–153.

[19] M.J. Hounslow, R.L. Ryall, V.R. Marshall, A discretized population balance for nucleation, growth and aggregation, AIChE J. 34 (1988) 1821–1832.